

# Dynamics of rotors in complex structures

N. Wagner, R. Helfrich

INTES GmbH, Stuttgart, Germany  
www.intes.de; info@intes.de

## Summary:

Rotating parts can be found in many mechanical products like in vehicles, airplanes, ships, machine tools. Because rotors are never perfect, imbalances are generating vibrations which not only excite the rotor itself but also other joint non-rotating parts. This coupling of rotating and non-rotating parts is an important point for virtual product development of parts with rotors.

First, the principles of modeling and analysis of rotors are revisited and usual post-processing features of rotor analysis results are shown. Second, an example for a joint structure with rotating and non-rotating parts is used to demonstrate the coupling effect. In particular, sound radiation from non-rotating parts due to imbalances of the rotor will be considered.

# 1 Introduction

Finite element technique has become a popular tool in rotordynamic analysis.

Dynamic studies of rotating machines are generally performed using, on the one hand, beam element models [11, 16] representing the position of the rotating shaft and, on the other hand, three-dimensional solid rotor-stator models [8, 13, 14]. Axisymmetric models are used by [11]. A specific advantage of solid models is the inclusion of stress stiffening, spin softening, and temperature effects in the rotor dynamics analysis. Nowadays CAD models of rotors becoming more and more detailed. The tedious and time-consuming task of building equivalent beam models is omitted by using solid models.

Rotor lateral vibration (sometimes called transverse or flexural vibration) is perpendicular to the axis of the rotor and is the largest vibration component in most high-speed machinery [10]. Understanding and controlling this lateral vibration is important because excessive lateral vibrations leads to bearing wear and, ultimately, failure. In extreme cases, lateral vibration also can cause the rotating parts of a machine to come into contact with stationary parts, with potentially disastrous consequences [10, 12].

All FEM computations are carried out in PERMAS [1]. PERMAS specific commands are highlighted by a preceding dollar sign and capital letters in the subsequent sections.

## 2 Governing Equations

Only linearized systems are considered here, i.e. only small variations of the rotational velocity is possible. Rotating systems may be processed in a stationary reference frame as well as a rotating reference frame.

In the following, we will focus on an inertial reference frame. The additional matrices due to rotating parts must be taken into account and are requested by a so-called \$ADDMATRIX data block within the \$SYSTEM block.

The complex eigenfrequencies of a rotor on fixed supports are determined. The structure is described with respect to a fixed reference frame, i.e. shaft and discs rotate with a constant rotational speed, whereas the bearings are supported and fixed to ground. All displacements, frequencies etc. refer to the fixed coordinate system. At one end, the rotation is suppressed to represent a drive with constant rotational speed.

The first computation step is a static analysis for the basic model to determine the stress distribution under centrifugal loads. It is a prerequisite for the calculation of the geometric stiffness matrix  $\mathbf{K}_g$ .

The next step is the calculation of real eigenmodes  $\mathbf{X} = [x_1 \dots x_r]$ , including geometric and convective stiffness matrices:

$$\mathbf{M}\mathbf{X} = (\mathbf{K} + \mathbf{K}_g + \mathbf{K}_c)\mathbf{X}\mathbf{\Lambda}, \quad \mathbf{\Lambda} = \begin{bmatrix} \lambda_1 & & \\ & \ddots & \\ & & \lambda_r \end{bmatrix}. \quad (1)$$

The governing equations of motion that describes a rotor system in a stationary reference frame is given by

$$\mathbf{M}\ddot{\mathbf{u}} + (\mathbf{D} + \mathbf{D}_b(\Omega) + \mathbf{G})\dot{\mathbf{u}} + (\mathbf{K} + \mathbf{K}_b(\Omega) + \mathbf{K}_g + \mathbf{K}_c)\mathbf{u} = \mathbf{R}(t), \quad (2)$$

where  $\mathbf{M}$  denotes the mass matrix,  $\mathbf{D}$  viscous damping matrix,  $\mathbf{D}_b(\Omega)$  speed-dependent bearing viscous damping matrix,  $\mathbf{G}$  gyroscopic matrix,  $\mathbf{K}_c$  convective stiffness matrix,  $\mathbf{K}_g$  geometric stiffness matrix,  $\mathbf{K}_b(\Omega)$  speed-dependent bearing stiffness matrix and

Material damping  $i\mathbf{H}$  of the stator is replaced by an equivalent viscous damping in the time-domain.

Including convective stiffness requires the use of a consistent mass matrix, which is the default formulation beginning with version 14.

The equations of motion (2) are transformed into modal space by means of

$$\mathbf{u} = \mathbf{X}\boldsymbol{\eta} \quad (3)$$

Additional pseudo mode shapes may be added to enrich the modal space. This is realized by \$ADDMODES.

$$\widetilde{\mathbf{M}}\ddot{\boldsymbol{\eta}} + (\widetilde{\mathbf{D}} + \widetilde{\mathbf{G}})\dot{\boldsymbol{\eta}} + (\widetilde{\mathbf{K}} + \widetilde{\mathbf{K}}_g + \widetilde{\mathbf{K}}_c)\boldsymbol{\eta} = \widetilde{\mathbf{R}}(t) \quad (4)$$

By introducing  $\zeta = \dot{\eta}$  the second order form (4) is transformed into a state-space form:

$$\begin{bmatrix} \widetilde{M} & \mathbf{O} \\ \mathbf{O} & \mathbf{I} \end{bmatrix} \begin{bmatrix} \dot{\zeta} \\ \dot{\eta} \end{bmatrix} + \begin{bmatrix} \widetilde{D} + \widetilde{D}_b + \widetilde{G} & \widetilde{K} + \widetilde{K}_g + \widetilde{K}_c \\ -\mathbf{I} & \mathbf{O} \end{bmatrix} \begin{bmatrix} \zeta \\ \eta \end{bmatrix} = \begin{bmatrix} \widetilde{R}(t) \\ \mathbf{0} \end{bmatrix} \quad (5)$$

To analyse rotating models two different coordinate systems can be used in PERMAS, stationary and rotating. By using a stationary reference frame the model can have both rotating parts and stationary parts. However, the rotation parts have to be axisymmetric. Moreover different components can rotate with different rotational speeds. A stationary reference frame is activated by

```
$ADDMATRIX
  GEOSTIFF CONVSTIFF GYRO
```

The rotational speed is defined in the loading definition of a static pre-run by \$INERTIA ROTATION. Additional matrices are build for that reference speed.

The modelling of a rotating machine requires a skew-symmetric pseudo-damping matrix named gyroscopic matrix. The particular form of the matrix makes complex eigenmodes appear, forward modes having increasing frequencies and backward modes having decreasing frequencies.

Critical speeds, stability and unbalance response were evaluated in the operating speed range.

## 2.1 Bearings

To a greater or lesser extent, all bearings are flexible and all bearings absorb energy. For most types of bearing, the load-deflection relationship is nonlinear. Furthermore, load deflection relationships are often a function of shaft speed. Speed-dependent bearings are idealized by CONTROL6 elements and multipoint constraints of type \$MPC WLSCON.

## 2.2 Damping

Identical damping specifications lead to different effects in fixed or co-rotating reference systems. In an inertial reference frame material damping is not suitable for rotating parts, whereas modal damping represents any kind of external damping. Discrete damping elements can be used for modelling damping in bearings.

## 2.3 Unbalance

In all rotating machinery, some degree of mass unbalance is always present. The unbalance load acts as a harmonic load in an inertial frame, i.e.

$$\begin{bmatrix} F_x \\ F_y \end{bmatrix} = m e \Omega^2 \begin{bmatrix} \cos \Omega t \\ \sin \Omega t \end{bmatrix}. \quad (6)$$

The balance quality grades for various groups of representative rigid rotors can be found in ISO 1940/1 and is defined as the product of a specific unbalance  $e$  in mm and the angular velocity  $\Omega$  in rad/s of the rotor at maximum operating speed:

$$G = e \Omega. \quad (7)$$

# 3 Examples

## 3.1 Gas Turbine

The first example is taken from the literature [9]. However we will use a solid model instead of a Timoshenko beam model. The solid model consists of 48372 hexahedra and 1000 pentahedra elements. Fig. 1 shows the mesh of the rotor model. The front and rear bearing are located at  $x = 0.04$  m and  $x = 0.7$  m, respectively. The rotor consists of 6 discs and a hollow shaft ( $l = 0.78$  m). Details concerning the physical and geometrical data can be found in [9].

VisPER (Visual PERMAS) is used for model validation and postprocessing tasks [3]. Medina is applied to generate the finite element mesh [5].

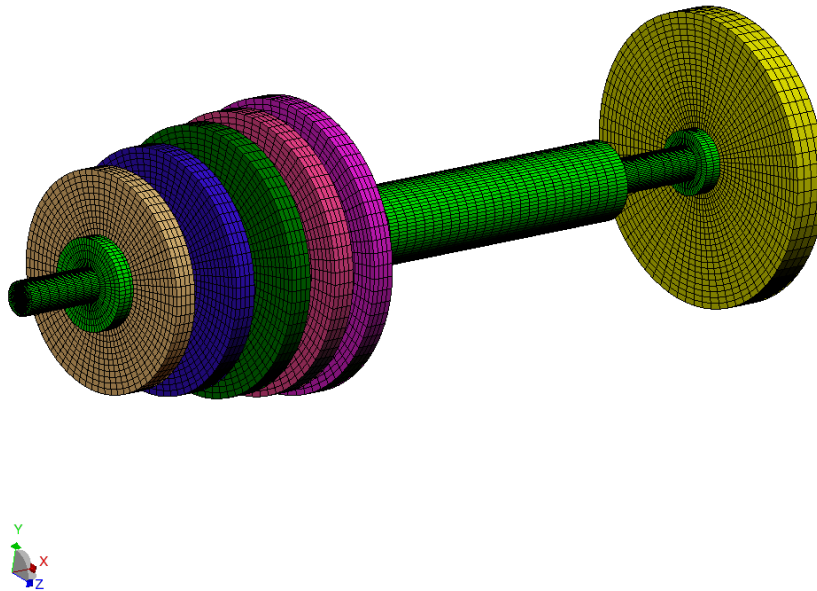


Fig. 1: Simplified rotor model of a gas turbine

Fig. 2 illustrates the characteristic of the frequency-dependent isotropic bearings.

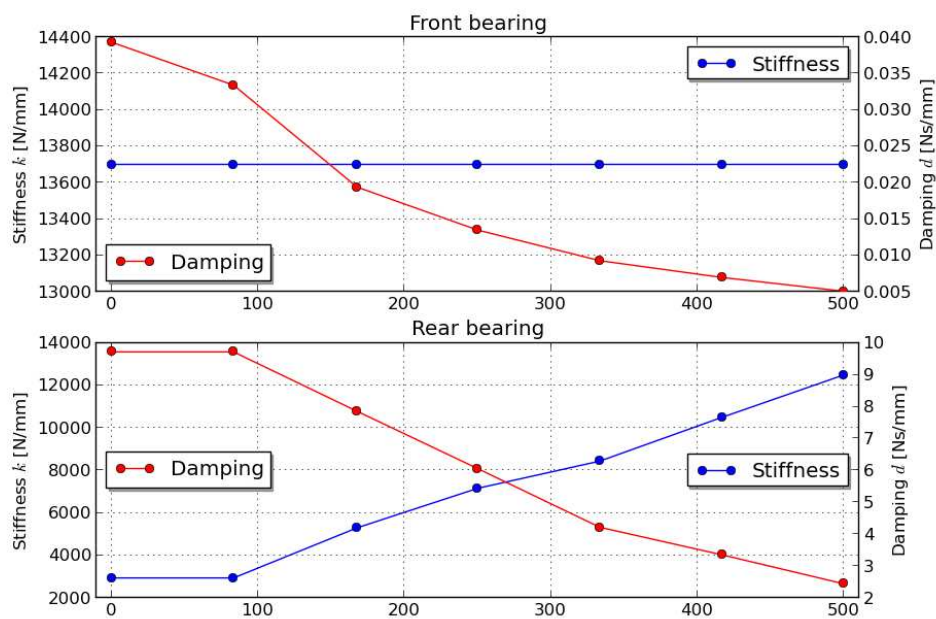


Fig. 2: Frequency-dependent coefficients of the bearings

### 3.1.1 Strain energy distribution

The strain energy distribution of the different parts of the rotor is illustrated in Fig. 3. Each column represents an eigenfrequency of the rotating system. Bending modes appear pairwise due to the symmetry of the rotor-bearing system. The third and sixth column represent torsional modes shapes. The first two bending modes are dominated by the rear bearing, whereas the front bearing participates in modes 4,5 and 7,8 respectively. Modes 11 and 12 exhibit axial modes of the shaft and discs. The elastic discs make a contribution to the strain energy density at higher modes, while the lower modes are dominated by the hollow shaft.

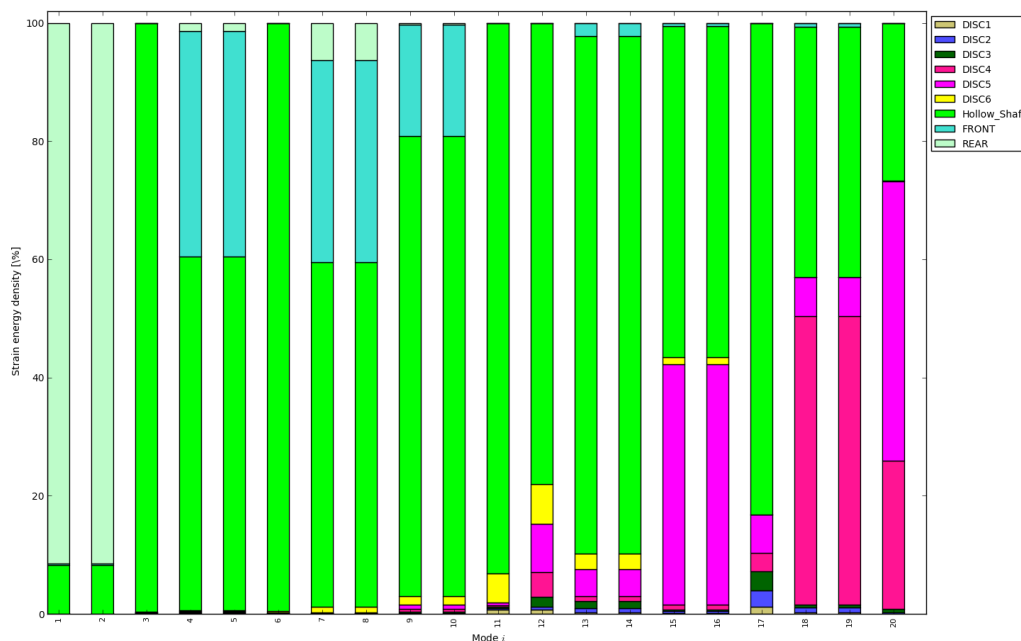


Fig. 3: Strain energy distribution

### 3.1.2 Campbell Diagram

In order to get the relation between eigenfrequencies and rotational speed an automatic procedure called \$MODAL ROTATING is available which directly generates all eigencurves. A mode tracking algorithm is implemented in order to sort the complex eigenvalues.

The Campbell diagram is depicted in Fig. 5. Solid lines denotes the eigencurves computed by PERMAS while the dash-dot lines corresponds to the beam model studied in [9]. Torsional modes are not present in the beam model. Besides the 3rd forward whirl all eigencurves are in good accordance with the results of the beam model. However, they share the feature of a strong variation with increasing rotor speed. The deviations within the Campbell diagram can be explained by the different modeling approaches. The beam model tends to be stiffer than the solid model especially for higher modes.

The first critical speed corresponding to the first forward whirl (FW) is at 51 Hz and a second critical speed related to the second forward whirl is at  $f = 150$  [Hz].

Nelson [15] showed that the backward mode vector is orthogonal to the unbalance vector and, as such, energy cannot be fed into the backward whirl. Therefore, critical speeds are restricted to forward whirl in case of symmetric rotors.

In order to judge the stability, the equivalent damping ratio

$$\xi_j = -\frac{\delta_j}{\sqrt{\delta_j^2 + \omega_j^2}} \quad (8)$$

is evaluated. The system is stable, if  $\xi_j > 0 \forall j$ . This condition is obviously satisfied here (s. Fig 4).

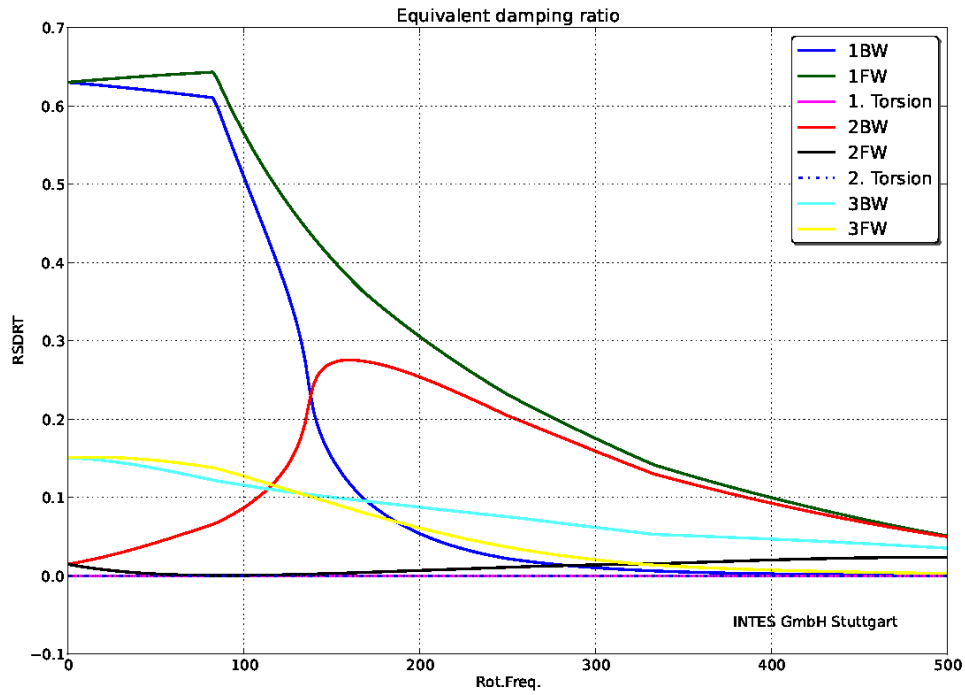


Fig. 4: Equivalent damping ratio of the rotor-bearing system

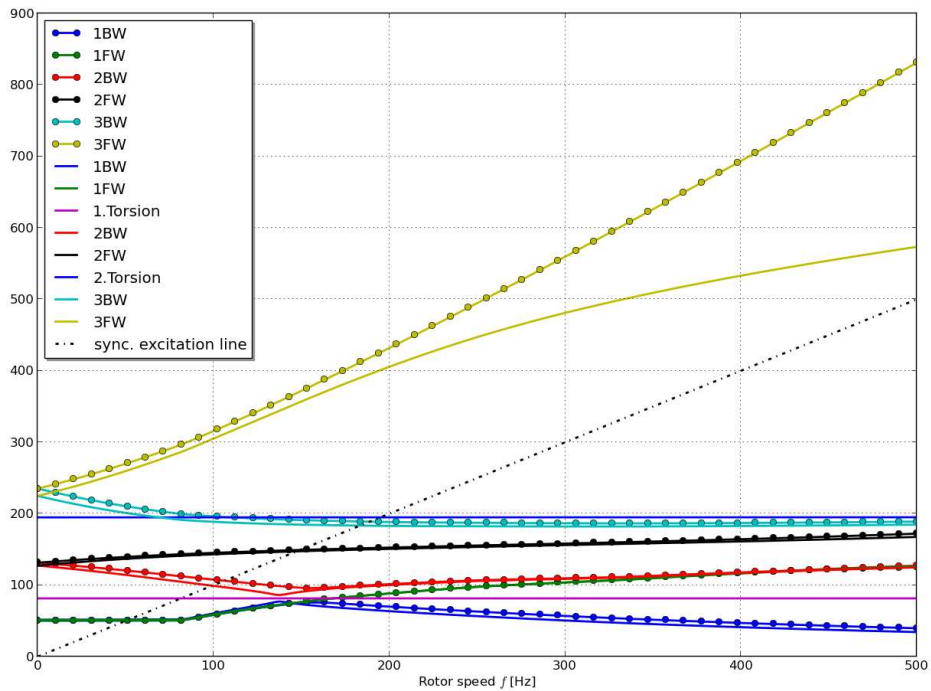


Fig. 5: Campbell Diagram of the rotor-bearing system

### 3.1.3 Unbalance

A mass unbalance of  $10^{-4}$  kg m situated at the single disc at node 21 of the finite element model is applied in the numerical analyses. Fig. 6 illustrates the amplitudes due to a mass unbalance at different nodes. The peak corresponding to the first critical speed is missing, since the damping of the rear bearing (Fig. 2) attenuates the response.

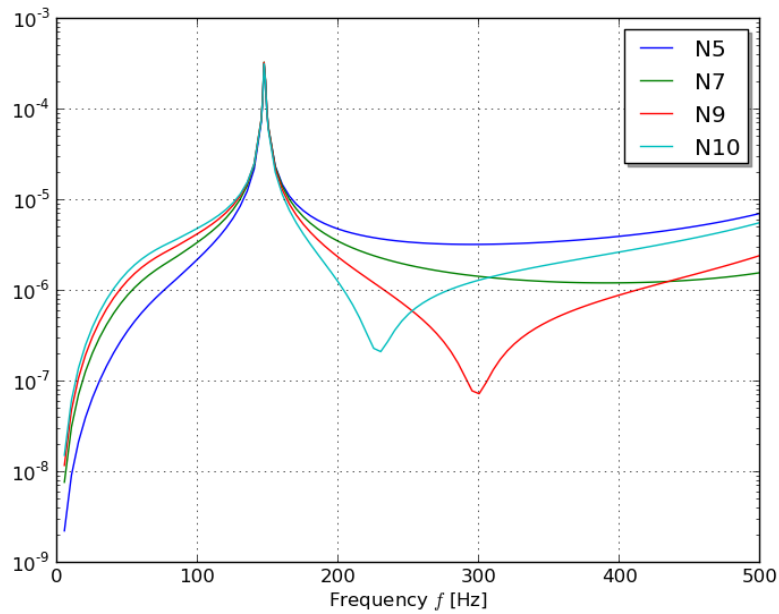


Fig. 6: Unbalance responses at certain nodes of the rotor-bearing system

The dynamic reaction forces of the bearings are depicted in Fig. 7

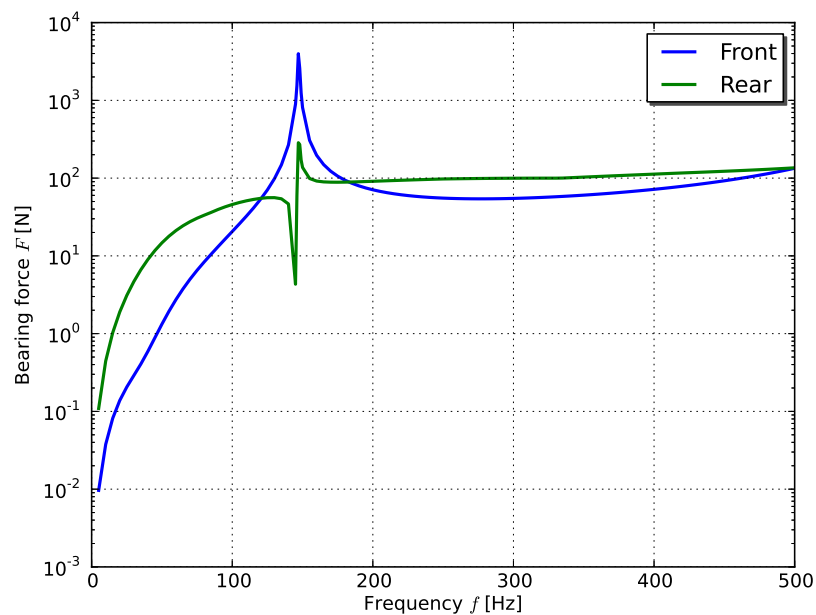


Fig. 7: Dynamic bearing forces

### 3.2 Bench grinder

A bench grinder is a type of benchtop grinding machine used to drive abrasive wheels [7]. Depending on the grade of the grinding wheel it may be used for sharpening cutting tools such as lathe tools or drill bits.

Alternatively it may be used to roughly shape metal prior to welding or fitting. Grinding wheels designed for steel should not be used for grinding softer metals, like aluminium. The soft metal gets lodged in the pores of the wheel and expand with the heat of grinding. This can dislodge pieces of the grinding wheel.

The CAD model of the bench grinder is available through Grabcad [6].

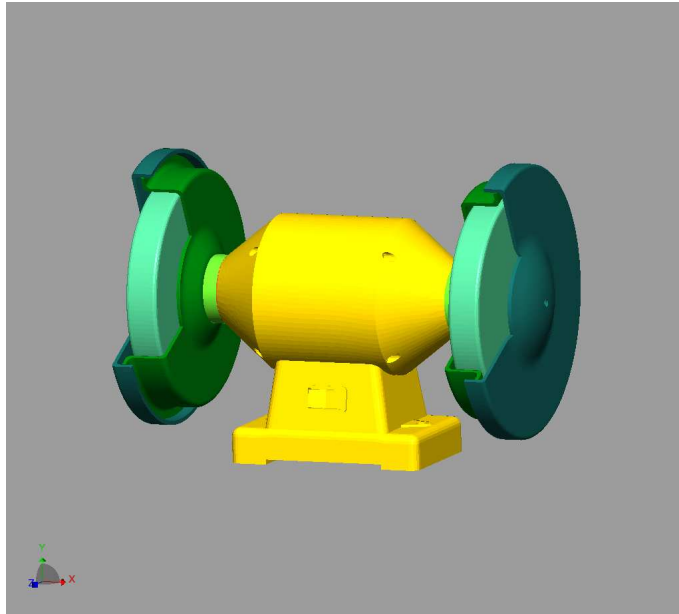


**Fig. 8: Bench grinder: Diameter of grinding wheel  $D = 123\text{mm}$**

It is an established fact that the casing has an effect on the dynamics of a rotor. Therefore, the interaction between the dynamics of the rotor with that of the casing is an essential aspect of the rotor dynamics. Therefore, all analyses are performed for the coupled system including the non-rotating and rotating part, respectively.

#### 3.2.1 Speed-dependent bearings

A diagonal stiffness matrix

$$\mathbf{K}_b(\Omega) = \text{diag} [ f_{2001}(\Omega) \quad f_{2002}(\Omega) \quad f_{2002}(\Omega) \quad 0 \quad 10^5 \quad 10^5 ] \quad (9)$$

is assumed for the bearings - hence cross coupling effects are neglected. The functions  $f_{2001}$ ,  $f_{2002}$  in equation (9) are illustrated in Fig. 9.

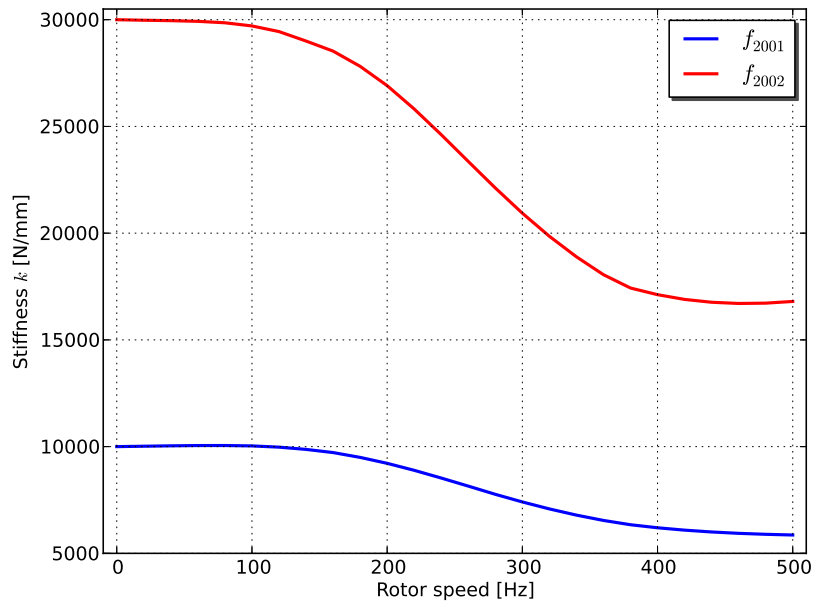


**Fig. 9: Speed-dependent bearing stiffness**

In addition a constant viscous damping matrix

$$D_b = \text{diag} [ 0.5 \quad 1.0 \quad 1.0 \quad 1.e - 5 \quad 2.0 \quad 2.0 ] \quad (10)$$

is used within the simulations.

The unbalance forces are assumed to be concentrated forces at the center of gravity of each grinding wheel.

### 3.2.2 Centrifugal load

The displacement under centrifugal loads is illustrated in Fig. 10. The static pre-run is necessary to compute the additional matrices due to rotation.

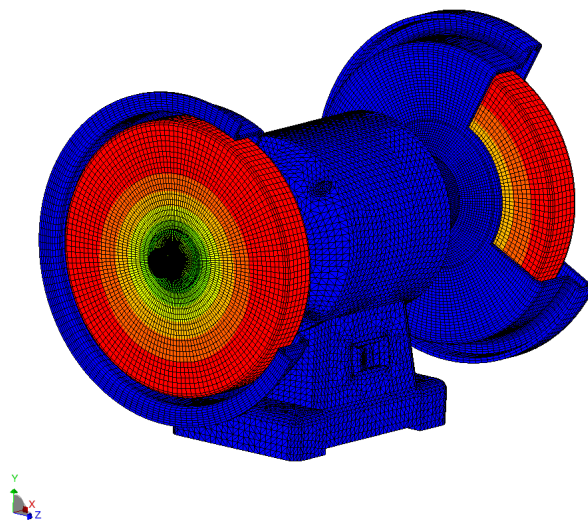


**Fig. 10: Displacement field due to a centrifugal load**

The Campbell diagram is shown in Fig. 11

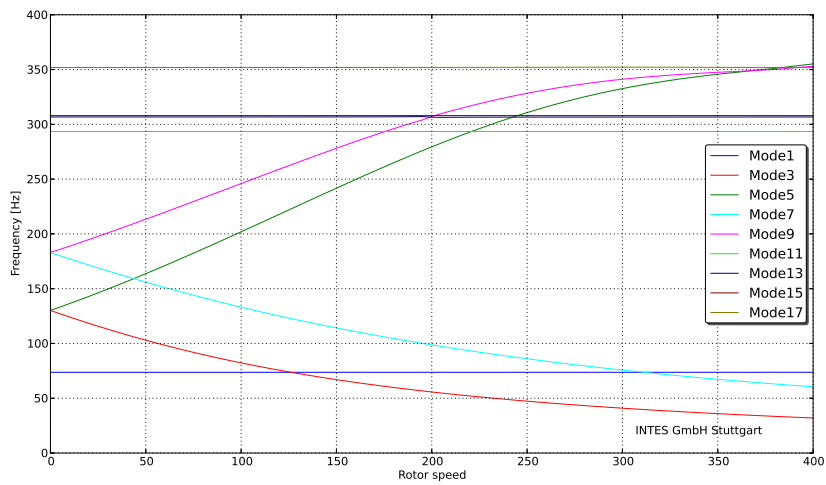


Fig. 11: Campbell diagram of the bench grinder

### 3.2.3 Sound radiation

Sound radiation power (densities) may be computed after an eigenvalue analysis, a frequency response or a time history analysis in PERMAS. The results are generated for all shell, membrane, so-called LOADA and FSINTA elements. The sound radiation power density is proportional to

$$\bar{v}^2 = \frac{1}{A} \int v_n^2 dA, \quad (11)$$

where  $v_n$  is the normal velocity of the vibrating surface. The result is the mean square value of the element velocity normal to the element surface.

The unbalance response of the bench grinder is presented at 50 cycles/s (s. Fig 12).

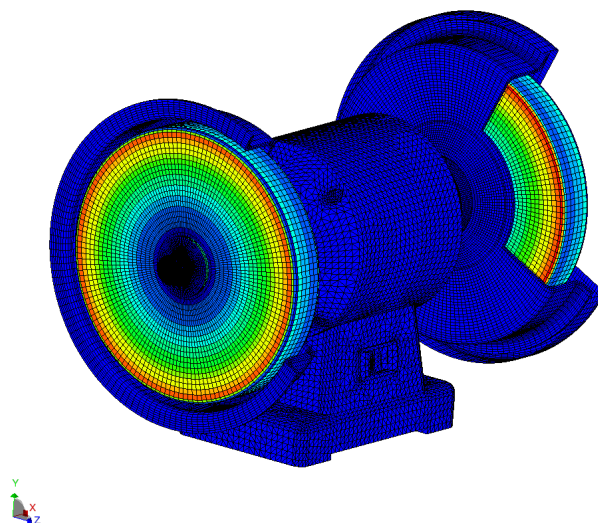


Fig. 12: Sound radiation power density at  $f = 50.0$  [Hz]

## 4 Conclusions

A complete rotor dynamic analysis was successfully performed and verified by an example from the literature. Typical results such as Campbell diagram, dynamic bearing forces due to an unbalance load, and critical speeds were evaluated. The second example addressed the rotor-stator interaction of a bench grinder. In addition the sound radiation power is computed for rotating and non-rotating parts of the structure.

Possible extensions of the presented material include:

- Design of lightweight rotating structures at high speeds requires a deep knowledge of rotordynamics to avoid excessive vibration in the operating speed range. For this reason it becomes obvious to use optimization techniques [17] in order to reduce stresses, displacements, etc. For this purpose PERMAS provides different modules such as topology, sizing and shape optimization. Various design constraints like \$DCONSTRAINT WEIGHT, \$FREQ, \$CAMPBELL, \$CFREQ, \$NPSTRESS, \$ELSTRESS are available to optimize the structure with regard to the above-mentioned constraints without the need to integrate an external optimizer in the process chain. Furthermore a positioning optimization is disposable.
- Further aspects such as critical speed maps, where the critical speeds are plotted as a function of the bearing stiffness in a semi-logarithmic manner, are important for a better understanding of rotor-bearing systems.

## 5 Acknowledgment

The authors would like to thank Dr. João C. Menezes and Dr. Geraldo Creci Filho for providing the Campbell diagram of the first example.

## References

- [1] *PERMAS Version 14: Users' Reference Manual*, INTES Publication No. 450, Stuttgart, 2012.
- [2] *PERMAS Version 14: Examples Manual*, INTES Publication No. 550, Stuttgart, 2012.
- [3] *Visper Version 3.1.005: Visper Users Manual*, INTES Publication No. 470, Stuttgart, 2012.
- [4] *PERMAS Product Description Version 14*, INTES, Stuttgart, 2012, [http://www.intes.de/kategorie\\_unternehmen/publikationen](http://www.intes.de/kategorie_unternehmen/publikationen)
- [5] *Medina FEM Pre- and Post-Processing*, T-Systems International GmbH, <http://servicenet.t-systems.com/medina>
- [6] *Grabcad* <http://grabcad.com/library/bench-grinder>
- [7] *Bench grinder* [http://en.wikipedia.org/wiki/Bench\\_grinder](http://en.wikipedia.org/wiki/Bench_grinder)
- [8] D. Combesure, A. Lazarus: *Refined finite element modelling for the vibration of large rotating machines: Applications to the gas turbine modular helium reactor power conversion unit*, Journal of Sound and Vibration, Vol. 318, pp. 1262–1280, (2008).
- [9] G. Creci, J. C. Menezes, J. R. Barbosa, J. A. Corra: *Rotordynamic analysis of a 5-kilonewton thrust gas turbine by considering bearing dynamics*, Journal of Propulsion and Power, Vol. 27, pp. 330–336, 2011.
- [10] M. I. Friswell, J. E. T. Penny, S. D. Garvey, A. W. Lees: *Dynamics of rotating machines*, Cambridge University Press, 2010.
- [11] M. Geradin, N. Kill: *A new approach to finite element modelling of flexible rotors*, Eng. Comput., Vol. 1, pp. 52–64, 1984.
- [12] G. Jacquet-Richardet, M. Torkhani, P. Cartraud, F. Thouverez, T. Nouri Baranger, M. Herran, C. Gibert, S. Baquet, P. Almeida, L. Peletan: *Rotor to stator contacts in turbomachines. Review and application*, Mechanical Systems and Signal Processing, in press, (2013).
- [13] A. Nandi, S. Neogy: *Modelling of rotors with three-dimensional solid finite elements*, Journal of Strain Energy, Vol. 36, pp. 359–371, 2001.
- [14] A. Nandi: *On computation of response of a rotor in deformed configuration using three-dimensional finite elements*, Communications in Numerical Methods in Engineering, Vol. 19, pp. 179–195, 2003.
- [15] F. C. Nelson: *Rotor dynamics without equations*, International Journal of COMADEM, Vol. 10, pp. 2–10, 2007.
- [16] H. D. Nelson: *A finite rotating shaft element using Timoshenko beam theory*, Journal of Mechanical Design, Vol. 102, pp. 793–803, 1980.
- [17] A. O. Pugachev, A. V. Sheremetyev, V. V. Tykhominov, I. D. Timchenko: *Gradient-based optimization of a turbo-prop rotor system with constraints on stresses and natural frequencies*, 51st AIAA/ASME/ASCE/AHS/ASC Structures, Structural Dynamics, and Materials Conference, 12–15 April 2010, Orlando, Florida.
- [18] M. B. Wagner, A. Younan, P. Allaire, R. Cogill: *Model reduction methods for rotor dynamic analysis: A survey and review*, International Journal of Rotating Machinery, Vol. , 2010.

[19] PERMAS Version 14: Rotierende Systeme  
[http://www.intes.de/kategorie\\_permas/anwendungen/rotierende\\_systeme](http://www.intes.de/kategorie_permas/anwendungen/rotierende_systeme)